Rapid #: -19643551

CROSS REF ID: **42685820120001591**

LENDER: **KKS :: Main Library**

BORROWER: **LIP :: Main Library**

TYPE:	Article CC:CCL
JOURNAL TITLE:	Journal de physique. III
USER JOURNAL TITLE:	JOURNAL DE PHYSIQUE III
ARTICLE TITLE:	THEORY OF OXYGEN TRACER DIFFUSION ALONG GRAIN-BOUNDARIES AND IN THE BULK IN 2-STAGE OXIDATION EXPERIMENTS .2. ANALYSIS OF TYPE-B REGIME
ARTICLE AUTHOR:	MISHIN, YM;BORCHARDT, G;
VOLUME:	3
ISSUE:	5
MONTH:	
YEAR:	1993
PAGES:	945-960
ISSN:	1155-4320
OCLC #:	

Processed by RapidX: 10/5/2022 9:20:47 AM

J. Phys. III France 3 (1993) 945-960 MAY 1993, PAGE 945

Classification
Physics Abstracts
66.30 — 81.60B

Theory of oxygen tracer diffusion along grain boundaries and in the bulk in two-stage oxidation experiments. Part II : analysis of type B regime

Yu. M. Mishin (*) and G. Borchardt

Sonderforschungsbereich 180 and Institut für Allgemeine Metallurgie, Technische Universität Clausthal, Robert-Koch-Str. 42, D-3392 Clausthal-Zellerfeld, Germany

(*Received 14 September 1992, accepted 4 February 1993*)

Abstract. — In part I of this work a model of ^{18}O transport in a growing oxide film with parallel grain boundaries has been proposed, and analysis of type A and type C regimes has been carried out. In this paper the analysis is extended to the intermediate, type B regime. We derive an analytical solution of the model, which describes both B and C type regimes as particular cases, and calculate tracer penetration profiles along grain boundaries depending on the drift velocity and time. The results of penetration profile analysis are presented as kinetic diagrams allowing to predict kinetic regimes of ^{18}O transport under various conditions. We also discuss methods of profile processing for diffusion parameters determination. The analytical solutions obtained and the kinetic diagrams constructed can be used for the treatment of experimental profiles measured in two-stage oxidation experiments.

1. Introduction.

In part I of this work [1] we have proposed a model for ^{18}O diffusion in a growing metal oxide film during the second stage of a two-stage oxidation experiment. In the model, the oxide film is bounded by two parallel interphase boundaries, oxide/gas and oxide/metal, and contains an array of grain boundaries (GBs) that are normal to the interphases and parallel to one another (Fig. 1). ^{18}O penetration into the film is described by two simultaneous differential equations with appropriate boundary conditions (Eqs. (18-23), (31) and (32) in [1]). The equations look more or less like the basic equations of Fisher's model for GB diffusion [2-5] but differ from those in two respects : first, the equations of reference [1] generally include drift terms (additional to normal diffusion terms) both for bulk (lattice) and GB transport. Consequently,

(*) *Permanent address :* Russian Institute of Aviation Materials, 17 Radio Street, 107 005 Moscow, Russia.

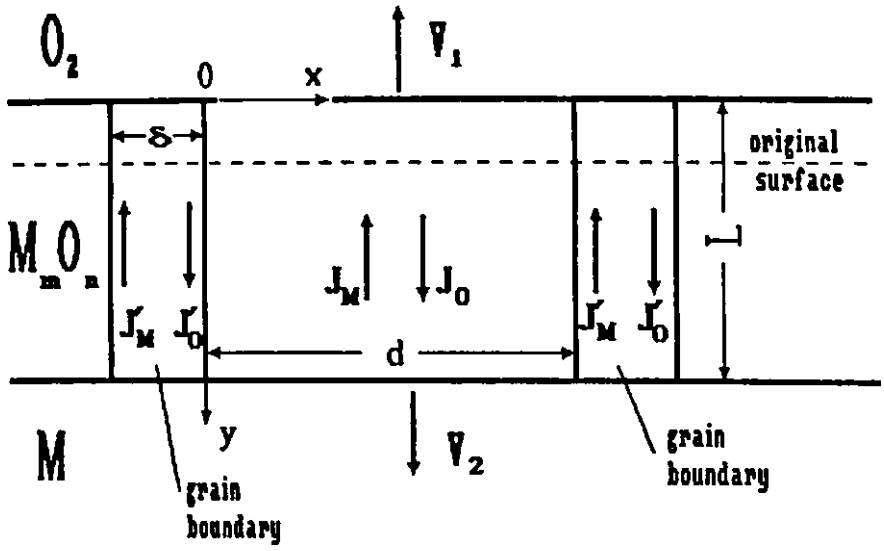

Fig. 1. — Schematic geometry in the model of oxide film growth in two-stage oxidation experiments. After reference [1].

each kind of transport may occur either in the pure diffusion regime or in the drift regime depending on interrelation between the drift velocity and the corresponding diffusion coefficient. Second, whereas the Fisher model refers to a semi-infinite specimen, the model of reference [1] considers a film of a finite thickness L. Therefore finite-size effects should be taken into account as the GB penetration depth L' becomes comparable with the film thickness after the first stage of the two-stage oxidation experiment, $L(0)$. Later on, when formally $L' \gg L(0)$, the GBs retain in isotope equilibrium and work only as sources of tracer along with the specimen surface and the oxide/metal interface.

Part I considered two extreme cases : type A regime when the film behaves like a homogeneous medium with an effective diffusivity combined of GB and bulk diffusion coefficients, and type C regime when bulk diffusion is nearly frozen out and tracer loss from GBs is negligible. Practically, these two extremes pertain to relatively high and relatively low temperatures, respectively. In the present paper, part II, we shall consider an intermediate situation known in GB diffusion theory as B-regime [4-6]. In this regime $\delta \ll (Dt)^{1/2} \ll d/2$. The purpose will be to reveal the most important limiting cases of ^{18}O transport under B-regime conditions and to derive analytical solutions for such cases. A general picture of oxygen tracer penetration into the growing oxide will be represented in terms of kinetic diagrams showing velocity/time conditions of realizing various regimes. These diagrams, along with the obtained formulas for ^{18}O concentration profiles, can be useful in the theoretical treatment of the results of two-stage oxidation experiments.

2. Problem formulation.

In the system of reference fixed to the surface, oxygen tracer transport is described by the following equations [1]

$$\frac{\partial c'}{\partial t} = D' \frac{\partial^2 c'}{\partial y^2} + \frac{2D}{\delta} \left(\frac{\partial c}{\partial x} \right)_{x=0} - V' \frac{\partial c'}{\partial y}, \tag{1}$$

$$\frac{\partial c}{\partial t} = D \left(\frac{\partial^2 c}{\partial x^2} + \frac{\partial^2 c}{\partial y^2} \right) - V \frac{\partial c}{\partial y}. \tag{2}$$

Throughout this paper we use the same notations of variables as in part I (see also Fig. 1). In particular, c' and c are excess ^{18}O concentrations (fractions) in GBs and in the bulk, respectively, D' and D are the corresponding tracer diffusion coefficients. The drift velocities V' and V are related to oxygen and metal self-diffusivities in GBs (D'_O and D'_M) and in the bulk (D_O and D_M) by

$$V' = \frac{1}{kTL} \int_{\mu_L}^{\mu_0} \left\{ D'_O + \frac{n}{m} [\nu D'_M + (1 - \nu) D_M] \right\} d\mu , \tag{3}$$

$$V = \frac{1}{kTL} \int_{\mu_L}^{\mu_0} \left\{ D_O + \frac{n}{m} [\nu D'_M + (1 - \nu) D_M] \right\} d\mu , \tag{4}$$

where $\nu = \delta/(d + \delta)$ is the volume fraction of GBs. At $t = 0$, c instantaneously increases at the surface from zero to c_0 (excess ^{18}O fraction in the atmosphere) and remains $c_0 = \text{const.}$ at $t > 0$. Experimentally measured tracer profiles are represent the laterally averaged concentration, $A(y, t)$, as a function of depth y:

$$A(y, t) = \frac{1}{d + \delta} \left[c'(y, t)\, \delta + 2 \int_0^{d/2} c(x, y, t)\, dx \right] . \tag{5}$$

Based on the results for C-regime [1, 7], one can qualitatively predict general features of tracer profile behaviour in B-regime. These features are schematically illustrated by figure 2. The bulk penetration zone near the surface exhibits a region of isotope equilibrium ($c \simeq c_0$) followed by the isotope boundary (IB). The latter moves with the velocity V and is diffuse to a width about $(Dt)^{1/2}$ due to bulk isotope exchange. At a fixed moment of time, the thickness of the isotope equilibrium region, ΔL_0, depends both on D_O and on the rate of new oxide growth at the surface, which in turn is determined by the rate of metal ions supply to the surface (the terms in square brackets in equations (3) and (4)). In more detail, the profile shape in the bulk transport region depends on time. Tracer penetration into the bulk starts in a pure diffusion regime, when ΔL_0 is small compared with $(Dt)^{1/2}$. Then the bulk penetration region is manifested as an erfc-shape near-surface portion of the profile with a width $\simeq (Dt)^{1/2}$. Later on, the process switches over to the drift regime, in which ΔL_0 is large while the IB is relatively sharp ($\Delta L_0 \gg (Dt)^{1/2}$).

In any case, the bulk penetration part of the profile is followed by a region governed by rapid transport of the tracer along GBs. At first, its depth L' remains much smaller than the initial film thickness $L(0)$, and the GB tracer transport occurs in the same way as in a massive specimen (Figs. 2a, b). As soon as L' reaches $L(0)$, the tracer immediately spreads over the oxide/metal interface due to fast interphase diffusion and then diffuses from it back to the bulk. At the same time, the tracer is incorporated in the new oxide layer growing at the internal interface to the measure of oxygen supply to this interface. As a result, an inner isotope layer generally appears with a thickness ΔL_i (Fig. 2c). If oxide growth is dominated by metal outward diffusion, the inner isotope layer is nearly missing. However, even in this case a second ^{18}O peak of thickness at least $\simeq (Dt)^{1/2}$ can be detected near the oxide/metal interface, caused by backward lattice diffusion of the tracer. Noteworthy, in a general case the second IB is more diffuse than the first one due to the effect of GB diffusion (see Sect. 5 in [1] for more detail). With time, the ^{18}O-deficient zone between the inner and outer isotope layers is consumed as a result of bulk isotope exchange. Sooner or later full isotope equilibrium is attained with $c \simeq c_0$ throughout the film.

This picture of oxygen penetration can be simulated numerically on the basis of equations (1) and (2). The general analytical solution of these equations is hardly possible.

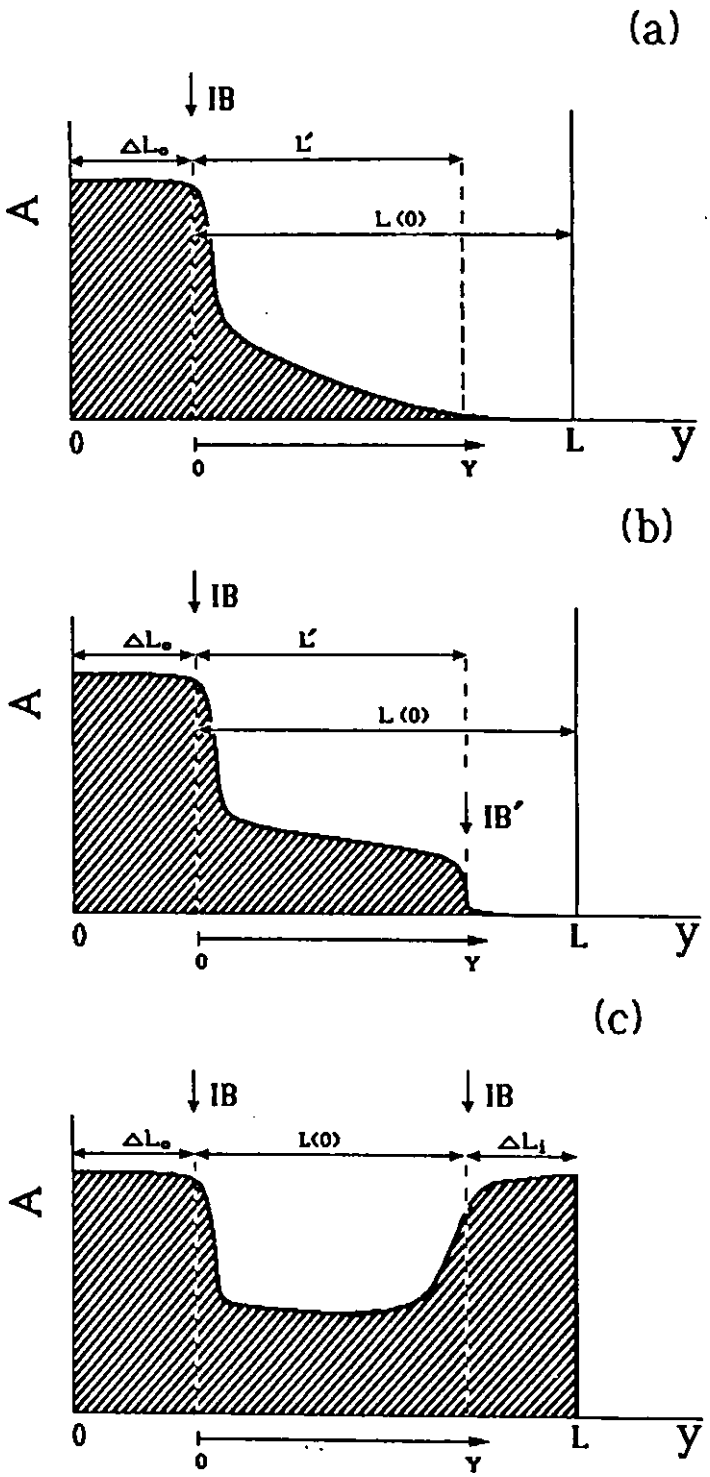

Fig. 2. — Schematic ^{18}O penetration profiles under B-regime conditions : (a, b) GBs are far from isotope equilibrium ; a) smooth GB-related tail ; b) step-like GB-related tail ; c) GBs are close to isotope equilibrium.

Therefore, in this paper we shall restrict the analysis to the following two particular but very important aspects of the problem :

(i) analysis of GB-related tails of the profiles, when $L' \ll L(0)$ (see Figs. 2a, b), and elaboration of methods for GB diffusion parameters determination ;

(ii) evaluation of the moment of attaining GB isotope equilibrium, when $L' \simeq L(0)$. This

moment is of great interest, since starting from it finite-size effects in the tracer transport should be taken into account and the second tracer concentration peak (near the oxide/metal interface) should generally appear.

For deriving analytical solutions for the GB-related tail of the profile we shall have to introduce three more simplifying assumptions.

Firstly, we suppose that the second stage of the oxidation experiment is shorter than the first one, $t \ll t_0$. Then, L in equations (3) and (4) approximately equals $L \simeq L(0) \equiv (2\,Kt_0)^{1/2} = \text{const.}$, and the drift velocities V and V' thus become time-independent. Secondly, we consider GBs in the GB diffusion zone ($y > \Delta L_0$) as isolated from each other. This can be the case whenever $(Dt)^{1/2} \ll d/2$, i.e. bulk diffusion fields around next-neighbouring GBs do not overlap. Thirdly, we assume that Le Claire's parameter $\beta = \frac{1}{2} D'\,\delta D^{-3/2}\,t^{-1/2}$ [4, 8] is large enough and therefore the term $\partial^2 c/\partial y^2$ in the bulk diffusion equation (2) can be left out. This implies that the GB penetration L' is great compared with the bulk diffusion path $(Dt)^{1/2}$ or, in other words, the IB in figures 2a, b is very sharp in the scale of L'.

Using the third assumption, it is convenient to come over to the frame of reference moving with the IB, or, mathematically, introduce a new coordinate $Y \equiv y - Vt$. Then, equations (1) and (2) in the GB diffusion zone ($Y > 0$) take the form

$$\frac{\partial c'}{\partial t} = D' \frac{\partial^2 c'}{\partial Y^2} + \frac{2\,D}{\delta} \left(\frac{\partial c}{\partial x} \right)_{x=0} - V_e \frac{\partial c'}{\partial Y}, \tag{6}$$

$$\frac{\partial c}{\partial t} = D \frac{\partial^2 c}{\partial x^2} \tag{7}$$

with boundary conditions

$$c(x, Y, 0) = 0\,, \quad c(x, 0, t) = c_0\,, \quad c(x, \infty, t) = 0\,,$$
$$c(\infty, Y, t) = 0\,, \quad c(0, Y, t) = c'(Y, t)\,. \tag{8}$$

In the new reference frame the tracer transport is represented by driven diffusion along GBs combined with drift-free bulk diffusion normal to GBs. The effective GB drift velocity equals

$$V_e = V' - V = \frac{1}{kTL} \int_{\mu_L}^{\mu_0} (D'_0 - D_0)\,\mathrm{d}\mu\,. \tag{9}$$

Thus, we have arrived at a final formulation of the problem to be solved analytically, equations (6-8).

Mathematically, equations (6-8) are similar to the basic equations for GB electromigration in thin films [9-13]. Moreover, Martin [10] and later Gupta, Campbell and Ho [9] used the same technique to eliminate the bulk drift term $V\,\partial c/\partial y$, namely, the variable change $Y = y - Vt$. It should be emphasized, however, that this technique is correct only when $\beta \gg 1$. Indeed, the new origin $Y = 0$ lies somewhere *inside* the bulk diffusion zone around the IB. If the latter is very sharp in the scale of L', which can be ensured by large β, the boundary condition $c = c_0$ at $Y = 0$ is a good approximation. If, however, the IB is highly diffuse ($\beta \simeq 1$ or $\ll 1$), the tracer concentration at $Y = 0$ can be essentially different from c_0 and the constant source condition $c(x, Y = 0, t) = c_0$ is no longer relevant.

3. Analytical solution.

To solve equations (6) and (7) with boundary conditions (8), let us first introduce the following reduced variables :

$$x_1 = \frac{x}{\delta}, \quad y_1 = \frac{Y}{\delta}\left(\frac{D}{D'}\right)^{1/2}, \quad t_1 = \frac{Dt}{\delta^2}, \quad V_1 = \frac{V_e\,\delta}{(DD')^{1/2}}. \tag{10}$$

Then, equations (6) and (7) take the form

$$\frac{\partial c'}{\partial t_1} = \frac{\partial^2 c'}{\partial y_1^2} + 2\left(\frac{\partial c}{\partial x_1}\right)_0 - V_1 \frac{\partial c'}{\partial y_1}, \tag{11}$$

$$\frac{\partial c}{\partial t_1} = \frac{\partial^2 c}{\partial x_1^2}. \tag{12}$$

For their solution, we shall apply the Laplace transformation method with respect to t_1 :

$$\bar{f}(p) = \mathcal{L}\{f(t_1)\} \equiv \int_0^\infty f(t_1)\exp(-pt_1)\,dt_1,$$

where the variable p is conjugate to t_1. This transformation reduces equations (11) and (12) to ordinary differential equations, which are solved for the Laplace image of the unknown solution, $\bar{c}(x_1, y_1, p)$, to give

$$\bar{c} = \frac{c_0}{p}\exp\left[\frac{1}{2}y_1 V_1 - y_1\left(\frac{1}{4}V_1^2 + p + 2p^{1/2}\right)^{1/2} - x_1 p^{1/2}\right]. \tag{13}$$

Recovering the original, corresponding to the image (13), is the most delicate step in the Laplace technique. The way chosen in reference [12] does not seem to be suitable : this leads to so complicated expressions that the resultant analytical solution can hardly be useful. (Notably, the authors of reference [12] preferred direct finite-difference solution of the basic equations to calculations from their analytical solutions). We shall apply a different method based on the Efros theorem. This approach has been very effective in deriving analytical solutions of GB diffusion problems [5, 14, 15].

Thus, the Efros theorem reads [16] : if

$$\bar{g}_0(p)\exp[-\tau\bar{q}(p)] = \mathcal{L}\{g(t_1, \tau)\}, \tag{14}$$

then

$$\bar{g}_0(p)\;\bar{R}[\bar{q}(p)] = \mathcal{L}\left\{\int_0^\infty R(\tau)\,g(t_1, \tau)\,d\tau\right\}. \tag{15}$$

The image (13) can be presented in the form $\bar{g}_0(p)\bar{R}[\bar{q}(p)]$ with

$$\bar{q}(p) = \frac{1}{4}V_1^2 + p + 2p^{1/2},$$

$$\bar{g}_0(p) = \frac{c_0}{p}\exp\left(\frac{1}{2}y_1 V_1 - x_1 p^{1/2}\right),$$

$$\bar{R}(p) = \exp(-y_1 p^{1/2}).$$

Then,

$$\bar{g}_0(p)\exp[-\tau\bar{q}(p)] = c_0 \exp\left(\frac{1}{2}y_1 V_1 - \frac{\tau}{4}V_1^2\right) \times \times \exp(-\tau p) \times \frac{1}{p}\exp[-(x_1 + 2\tau)p^{1/2}]. \quad (16)$$

Using the well-known transformation formula [17]

$$\frac{1}{p}\exp(-ap^{1/2}) = \mathcal{L}\left\{\operatorname{erfc}\left(\frac{a}{2t_1^{1/2}}\right)\right\}$$

and the translation theorem $\exp(-bp)\bar{f}(p) = \mathcal{L}\{H(t_1 - b)f(t_1 - b)\}$ [17], the image function (16) is inverted to

$$g(t_1, \tau) = c_0 H(t_1 - \tau)\exp\left(\frac{1}{2}y_1 V_1 - \frac{\tau}{4}V_1^2\right)\operatorname{erfc}\left[\frac{x_1 + 2\tau}{2(t_1 - \tau)^{1/2}}\right], \quad (17)$$

H being the Heaviside unit step function. On the other hand, $\bar{R}(p)$ is easily inverted to [17]

$$R(t_1) = \frac{y_1}{2\pi^{1/2}t_1^{3/2}}\exp\left(-\frac{y_1^2}{4t_1}\right). \quad (18)$$

Combining expressions (17) and (18) with the inversion formula (15), we get the original

$$c(x_1, y_1, t_1) = \frac{c_0 y_1}{2\pi^{1/2}}\int_0^{t_1}\exp\left(\frac{1}{2}y_1 V_1 - \frac{y_1^2}{4\tau} - \frac{\tau}{4}V_1^2\right) \times \operatorname{erfc}\left[\frac{x_1 + 2\tau}{2(t_1 - \tau)^{1/2}}\right]\frac{d\tau}{\tau^{3/2}}. \quad (19)$$

Introducing a new integration variable $\theta = y_1/2\tau^{1/2}$, expression (19) finally becomes

$$c(\xi, w, \alpha, \omega) = \frac{2c_0}{\pi^{1/2}}\int_{w\alpha^{1/2}/2}^{\infty}\exp\left[-\left(\theta - \frac{\omega}{\theta}\right)^2\right]\operatorname{erfc}(Z)\,d\theta, \quad (20)$$

where

$$Z \equiv \frac{(w^2/8\theta^2 + \xi/2)}{(1 - w^2\alpha/4\theta^2)}. \quad (21)$$

Here

$$\xi = \frac{x}{(Dt)^{1/2}}, \quad w = \frac{Y}{(D'\delta)^{1/2}}\left(\frac{4D}{t}\right)^{1/4} \text{ and } \alpha = \frac{\delta}{2(Dt)^{1/2}} \quad (22)$$

are traditional reduced variables of Fisher's model [2-5], whereas

$$\omega = YV_e/4D' \quad (23)$$

is a new, velocity-dependent variable.

Thus, we have derived the exact analytical solution of the model equations (6) and (7). Compared to the solution obtained in [12], our solution (20) is much simpler and more convenient for numerical calculations. In particular, it does not include the Bessel functions.

The tracer penetration profile is determined by averaging solution (20) according to formula (5). This yields

$$A(w, \alpha, \omega) = \frac{c_0 \nu}{\alpha \pi^{1/2}} \int_{w\alpha^{1/2}/2}^{\infty} \exp\left[- \left(\theta - \frac{\omega}{\theta} \right)^2 \right] \Phi \left(\frac{w^2}{4\theta^2}, \alpha \right) d\theta , \tag{24}$$

where the function $\Phi(z, \alpha)$ is given by

$$\Phi(z, \alpha) = (\alpha - 2z) \operatorname{erfc} \left[\frac{z/2}{(1 - z\alpha)^{1/2}} \right] + \frac{4(1 - z\alpha)^{1/2}}{\pi^{1/2}} \exp\left(- \frac{z^2/4}{1 - z\alpha} \right) . \tag{25}$$

Let us now consider practically important limiting cases of solution (20). First, suppose that the drift velocity V_e is vanishing, which corresponds to purely diffusion kinetics of GB tracer transport. Then, $\omega \to 0$ and equations (20-25) easily reduce to the standard solution of the Fisher model (cf. Eqs. (18) and (28) in [5]). This solution actually describes GB diffusion in two regimes : B and C. In B-regime $(Dt)^{1/2} \gg \delta$ and GB diffusion is quasi-steady, i.e. the term $\partial c'/\partial t$ in equation (6) can be omitted. Accordingly, by letting $\omega \to 0$ and $\alpha \to 0$ in equations (24) and (25) one obtains for the tracer profile [5]

$$A = \frac{2 c_0 \nu}{\alpha} \int_0^{\infty} \operatorname{erfc}(\theta) \operatorname{erfc} \left(\frac{w}{2\theta^{1/2}} \right) d\theta . \tag{26}$$

In the other extreme, when $\delta \gg (Dt)^{1/2}$ (i.e. $\alpha \to \infty$), we are in C-regime with an error-function profile

$$A = c_0 \nu \operatorname{erfc} \left[\frac{Y}{2(D' t)^{1/2}} \right] . \tag{27}$$

In this case the tracer diffuses along GBs without leakage to the bulk.

Now consider the other limiting case, where the drift velocity is very high. Then $\omega \to \infty$ and the exponential function in solution (20) has a very sharp maximum at $\theta_m = \omega^{1/2}$. Due to this feature, the integral in expression (20) can be evaluated by the saddle point method to give $c \simeq c_0 H(V_1 t_1 - y_1) \operatorname{erfc} [Z(\theta_m)]$, or, after rearrangement,

$$c = c_0 H(V_e t - Y) \operatorname{erfc} \left[\frac{Y/2(D_* t)^{1/2} + \xi/2}{(1 - Y/V_e t)^{1/2}} \right] , \tag{28}$$

where

$$D_* = V_e^2 \delta^2/4 D \tag{29}$$

is an effective GB diffusion coefficient. Solution (28) could be also obtained by omitting the term $D' \partial^2 c'/\partial Y^2$ in equation (6) and repeating the Laplace procedure. This solution describes ^{18}O penetration by the mechanism of GB drift. Again, there can be two extreme situations. At low temperature the tracer leakage from GBs is neglected and we are in a C-type regime with $\alpha \to \infty$. In that case solution (28) reduces to $c \simeq c_0 H(V_e t - Y) \operatorname{erfc} (\xi/2)$, or, for the penetration profile,

$$A = c_0 \nu H(V_e t - Y) . \tag{30}$$

The GB tail is thus step-like with a sharp isotope boundary IB' (see Fig. 2b). At higher

temperatures we arrive at a B-type regime with quasi-steady GB diffusion ($\alpha \to 0$). Then, solution (28) takes the form

$$c = c_0 \operatorname{erfc}\left[\frac{Y}{2(D_* t)^{1/2}} + \frac{\xi}{2}\right]. \tag{31}$$

The corresponding penetration profile is given by

$$A = \frac{2 c_0 \nu}{\alpha} \operatorname{ierfc}\left[\frac{Y}{2(D_* t)^{1/2}}\right], \tag{32}$$

where the integral error-function ierfc (x) is determined as

$$\operatorname{ierfc}(x) \equiv \int_x^\infty \operatorname{erfc}(x)\,dx = \pi^{-1/2} \exp(-x^2) - x \operatorname{erfc}(x).$$

In this regime the tracer also drifts along GBs to the measure of V_e, but due to extensive tracer leakage from GBs the average tracer concentration A (Eq. (5)) decays continuously with depth, resulting in a smooth penetration profile (32).

4. Kinetic analysis of GB tracer transport.

4.1 GRAIN BOUNDARIES FAR FROM ISOTOPE EQUILIBRIUM. — The above derived analytical solutions relate to the case when the GBs are far from isotope equilibrium, i.e. $L' \ll L(0)$. The general analytical solution for this case is given by equation (20). However, any real experiment most probably realizes one of the four extreme cases as considered above. Two of them, B-regime and C-regime, describe purely diffusion kinetics of GB tracer transport ($\omega \to 0$). In B-regime ^{18}O concentration decreases continuously with depth, whereas the characteristic penetration length L' grows with time as $L' \propto t^{1/4}$ (this law can be evaluated from the condition $w = 1$). The tracer penetration profile is determined by equation (26). When plotted in the coordinates ln A *versus* Y, the experimental profile (more exactly, its GB-related tail) should look more or less like a straight line or can show a slight downward curvature. Using the 6/5-method [4, 8] or more precise profile treatment techniques (e.g. [18]), one can determine the combination $D' \delta / D^{1/2}$ and then, knowing D from independent measurements, estimate the product $D' \delta$. In C-regime the tracer profile shows an erfc-shape (Eq. (27)) with the penetration law $L' \propto t^{1/2}$. Fitting the experimental profile Arg (erfc (A/A_0)) vs. Y by a straight line, one can extract the GB diffusion coefficient D' (here A_0 is the limit of A at $Y \to 0$).

In the other two regimes the tracer penetrates along GBs by the mechanism of GB drift ($\omega \to \infty$). Again, one can distinguish two essentially different situations. At low temperature ($\alpha \to \infty$) the tracer is not practically lost from GBs and a step-like penetration profile (30) results (see Fig. 2b). The isotope boundary IB' advances along the Y-axis with the velocity V_e, leaving behind a zone with isotope equilibrium in GBs ($c' \simeq c_0$). This C-type regime will be called driven C, or *DC-regime*. Having measured the coordinate of the IB', $L' = V_e t$, one can estimate V_e. At higher temperature ($\alpha \to 0$) we come to the other extreme : the tracer leakage is so extensive that it becomes the rate-controlling step of the tracer transport, like in normal B-regime. GB diffusion itself remains, however, strongly driven. As a result, a continuous ierfc-shape profile (32) arises with the effective diffusion coefficient D_* (Eq. (29)) combined of V_e (GB drift) and D (leakage to the bulk). This diffusion coefficient can be

determined from the experimental slope of the plot Arg (ierfc (A/A_0)) against Y. In this driven B-regime, which will be referred to as *DB-regime*, the penetration law is $L' \propto t^{1/2}$.

The results of this analysis are summarized as a kinetic diagram in figure 3. A situation is considered that D' is fixed while V_e can vary. At a fixed V_e, three kinetic regimes follow each other in time. The diagram shows, therefore, velocity-time conditions of realizing different regimes. The boundaries between the areas relating to different regimes were estimated by equating the GB penetration lengths, L', for these regimes. The necessary expressions for L' in terms of t and V_e are listed in table I. As it should have been expected, the C/B and DC/DB transitions occur at a moment $t = \delta^2/4\,D$ when the condition $\alpha = 1$ is met. The boundaries C/DC and B/DB are determined by equations $t = D'/V_e^2$ and $t = 4\,D\,(D')^2/\delta^2\,V_e^4$, respectively. The multiple (or critical) point M has the coordinates

$$t_* = \delta^2/4\,D \quad \text{and} \quad V_* = 2\,(DD')^{1/2}/\delta\,. \tag{33}$$

The diagram shows that independent of the drift velocity the tracer penetration always starts in C-regimes and ends up with DB-regime. The intermediate regime, however, depends on whether $V_e < V_*$ or $V_e > V_*$. If $V_e \ll V_*$ (poor drift conditions), at first the same sequence C → B is observed as in the standard Fisher model, but later, after a long time, B-regime changes for DB (unless the tracer earlier reaches the oxide/metal interface). In the present case the apparent diffusivity D_* in DB-regime is smaller than D'. Indeed, combining equations (29) and (33) one gets

$$(D_*/D') = (V_e/V_*)^2\,, \tag{34}$$

from which it follows that $D_* \ll D'$ provided $V_e \ll V_*$.

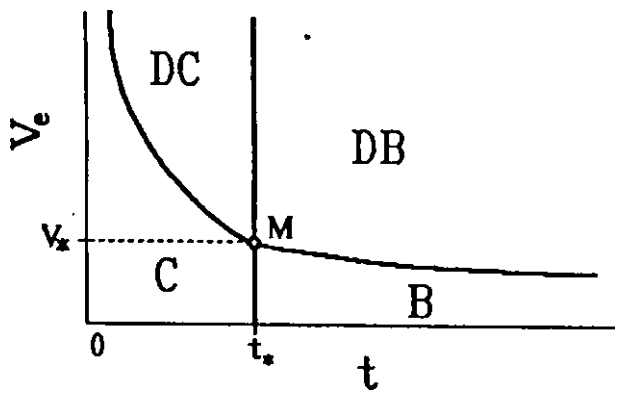

Fig. 3. — Kinetic diagram of oxygen tracer transport along GBs in a growing oxide film without finite-size effects. The diagram shows schematically velocity-time conditions of realizing purely diffusion (B and C) and driven (DB and DC) regimes of transport. Coordinates of the multiple point M are given by equation (33).

Table I. — *Characterization of* ^{18}O *transport regimes along GBs in a growing oxide film.*

Regime	α	ω	L'
B	$\ll 1$	$\ll 1$	$(D'\,\delta)^{1/2}\,(t/4\,D)^{1/4}$
C	$\gg 1$	$\ll 1$	$(D'\,t)^{1/2}$
DB	$\ll 1$	$\gg 1$	$(D_*\,t)^{1/2}$
DC	$\gg 1$	$\gg 1$	$V_e\,t$
E	—	—	$\gg L(0)$

If $V_e \gg V_*$ (strong drift), C-regime occurs only for a very short time, after which it changes to DC. With time the tracer leakage from GBs becomes more and more pronounced, the step-like profile becomes diffuse and finally, after a time $t > t_*$, we enter DB-regime with $D_* \gg D'$ (the latter relation follows from Eq. (34)). Lastly, at $V_e = V_*$ the tracer first diffuses in C-regime and then (at $t = t_*$) changes directly to DB-regime. This latter transition is accompanied only by a slight change in the profile shape, from erfc to ierfc, whereas the diffusion coefficient remains the same (according to Eq. (34) $D_* = D'$ when $V_e = V_*$).

The discussed features of profile behaviour are illustrated by numerical calculations, the results of which are presented in figure 4. The profiles were computed from the exact expression (24) using an adaptive integration procedure. For convenience, the profiles are shown in the coordinates A/A_0 against the reduced depth y_1 for various values of t/t_* and V/V_*. Here

$$A_0 \equiv \lim_{\gamma \to 0} A = \frac{2 c_0 \nu}{\alpha \pi^{1/2}} \left(1 + \frac{\alpha \pi^{1/2}}{4}\right).$$

The profiles in figure 4a ($V_e = 0.1\ V_*$) correspond to poor drift conditions, which fact can be seen from their erfc-like or exp-like shape. By contrast, the profiles in figure 4b are strongly driven ($V_e = 100\ V_*$). In this case the penetration depths are much greater (note different scales of y_1 between Figs. 4a and 4b) and the DC-regime profiles ($t < t_*$) exhibit the characteristic step-like shape. To demonstrate this more clearly, several DC-profiles are shown separately in figure 4c. One can observe how the step diffuses as we approach the DC/DB transition occurring at $t \simeq t_*$.

The above analysis and the diagram in figure 3 demonstrate that kinetics of ^{18}O penetration along GBs critically depends on the ratio V_e/V_*. Let us evaluate this ratio. Since $D'_O \gg D_O$, expression (9) for V_e approximately equals

$$V_e \simeq \frac{1}{kTL} \int_{\mu_L}^{\mu_0} D'_O \, d\mu . \tag{35}$$

Under well-known simplifying assumptions [19], equation (35) integrates to

$$V_e \simeq (1 + z) D'_O / L , \tag{36}$$

where z is the effective charge of the oxygen ions. In equation (36) D'_O means the oxygen self-diffusivity at the surface in case of the interstitial mechanism of oxygen transport, or at the oxide/metal interface in case of the vacancy mechanism. This difference is highly essential, because the values of D'_O at these two interfaces usually differ by orders of magnitude. Importantly, in the present model the values of D and D' refer to the surface [1].

If oxygen transport is dominated by the interstitial mechanism, the estimate (36) becomes

$$V_e \simeq (1 + z) D'/f' L , \tag{37}$$

f' being the correlation factor for GB tracer diffusion. Then, by virtue of equation (33) one finds

$$\frac{V_e}{V_*} = \frac{(1 + z)}{2 f'} \left(\frac{D'}{D}\right)^{1/2} \times \frac{\delta}{L} . \tag{38}$$

This relation shows that the fraction V_e/V_* is determined by the competition between two independent factors, $(D'/D)^{1/2} \gg 1$ and $\delta/L \ll 1$, the result of which can hardly be predicted *a*

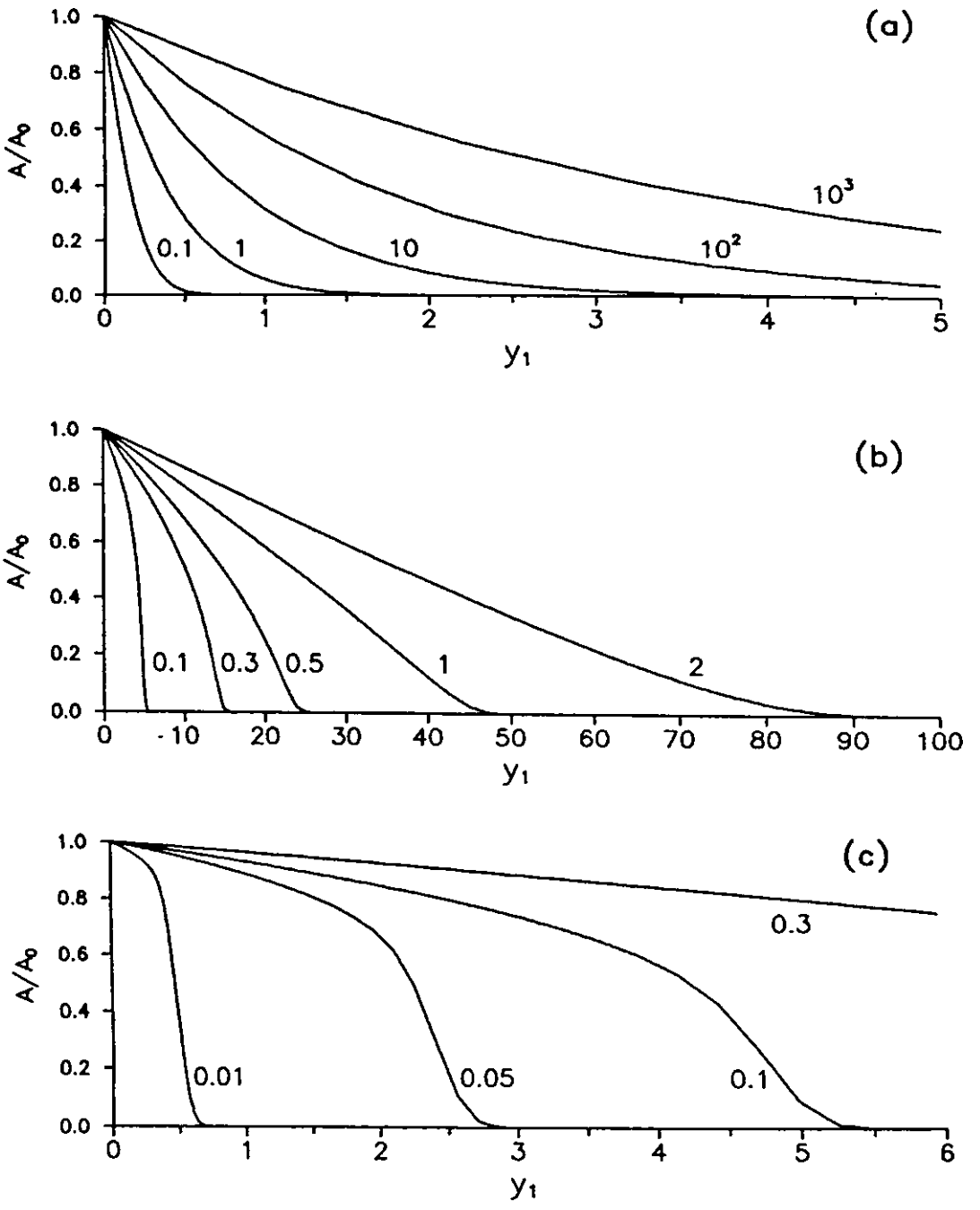

Fig. 4. — GB-related portions of ^{18}O penetration profiles as calculated from the exact analytical solution (Eqs. (24) and (25)). The profiles are shown in the coordinates A/A_0 against the reduced depth y_1 for $V_e/V_* = 0.1$ (a) and 100 (b, c) for selected values of t/t_*.

priori. If $D'\,\delta^2 \gg DL^2$, we have $V_e > V_*$ and GB tracer transport is strongly driven (see Figs. 4b, c). If $D'\,\delta^2 \ll DL^2$, $V_e < V_*$ and the tracer transport is virtually drift-free, like in Fisher's model (see Fig. 4a). At a fixed L, the situation shifts towards more strongly driven transport as the temperature decreases.

In case of the vacancy mechanism D'_O in equation (36) is much greater than D'. Consequently, the ratio V_e/V_* is considerably higher than it is predicted by relation (38), and thus the driven regimes DC and DB are more likely to be found. In other words, the vacancy mechanism strongly favours the tracer drift along GBs.

4.2 GRAIN BOUNDARIES CLOSE TO ISOTOPE EQUILIBRIUM. — Thus far, we have been restricted to consider the situation when finite size effects can be neglected. In C-regime the distance between the IB and the oxide/metal interface equals the initial film thickness $L(0)$ [1]. Up to corrections of order $(Dt)^{1/2}$, this obviously applies to the type B regime (see Figs. 2a, b). Therefore, the condition for neglecting finite size effects is $L' \ll L(0)$. In the other limit, when $L' \gg L(0)$, the GBs are nearly in isotope equilibrium (see Fig. 2c). The moment t of transition to GB isotope equilibrium can be estimated from the equation $L'(t) = L(0)$. The purpose of this section is to modify the above analysis by taking into account the possibility of this transition. In other words, we shall formally consider GB isotope equilibrium as one more kinetic regime (let us call it *E-regime*) and determine the field relating to this regime on the kinetic diagram in figure 3. After this revision the diagram will make it possible to predict, at least qualitatively, the time of the second isotope peak appearance at the profile, depending on the drift velocity, temperature, or other factors.

It is obvious *a priori* that the resultant diagram should depend on $L(0)$. Moreover, it turns out that a critical film thickness exists, L_*, such that the diagrams for $L(0) < L_*$ and $L(0) > L_*$ look radically different. These two types of diagram are shown schematically in figure 5 in terms of the reduced variables

$$\tau = t/t_*, \quad \Omega = V_e/V_*, \quad \lambda = L(0)/L_* . \tag{39}$$

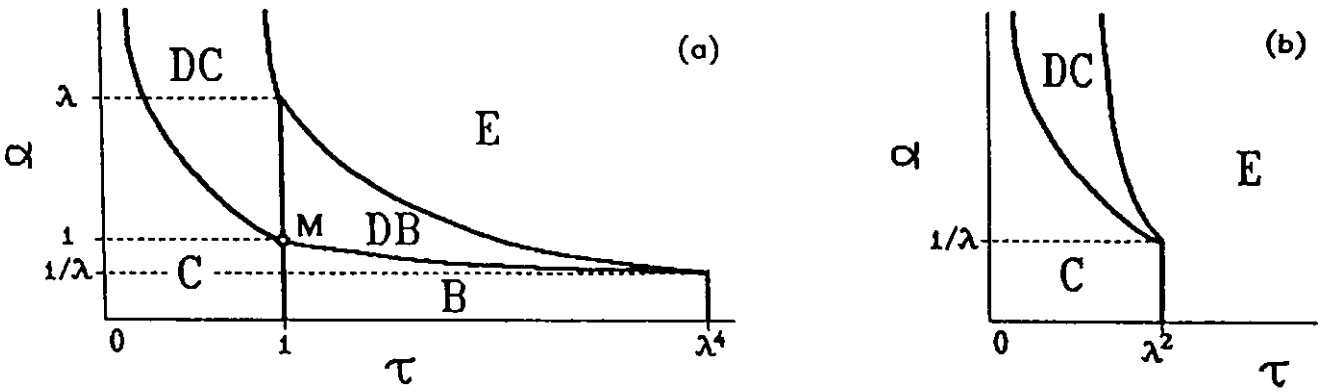

Fig. 5. — Kinetic diagram of oxygen tracer transport along GBs in a growing oxide film, including finite-size effects. The diagram shows schematically velovity-time conditions of realizing purely diffusion regimes (B and C), driven regimes (DB and DC), and GB isotope equilibrium (E). a) for a thick film ($\lambda > 1$); b) for a thin film ($\lambda < 1$).

(Thus, the multiple point in Fig. 3 has the coordinates $\tau = 1$ and $\Omega = 1$). To be short, oxide films with $L(0) > L_*$ (i.e. $\lambda > 1$) and $L(0) < L_*$ (i.e. $\lambda < 1$) will be referred to as *thick films* and *thin films*, respectively.

To understand the origin of the critical film thickness L_*, let us consider a particular case that $V_e = 0$. In this case the tracer starts penetration along GBs in C-regime and at $t \simeq t_*$ can switch to B-regime. Then later, at a moment $t' > t_*$ the condition $L'(t') = L(0)$ is met indicating the transition B/E. Using $L'(t)$ for B-regime (see Tab. I), t' equals

$$t' = 4\, DL(0)^4/(D'\,\delta)^2 . \tag{40}$$

However, if the film is thin enough, the GB isotope equilibrium can be attained before the moment t_*, i.e. while we are still in C-regime. Then, the C/B transition is not actually observed, whereas the C/E transition occurs at a moment t'' such that $L'(t'') = L(0)$ and $t'' < t_*$. Using $L'(t)$ for C-regime (see Tab. I), we find

$$t'' = L(0)^2/D' . \tag{41}$$

Thus, the tracer penetration scenario can be either C → B → E for a thick film or just C → E for a thin film. Therefore, the critical film thickness can be determined from the condition $t' = t'' = t_*$. Combining equations (40) and (41), this condition yields

$$L_* = \frac{1}{2}\,\delta\,(D'/D)^{1/2}\,. \tag{42}$$

The same appears to be true for $V_e \neq 0$. In thin films B-type regimes (B and DB) never occur (see Fig. 5b) and we come to GB isotope equilibrium either directly from C-regime (when $\Omega < 1/\lambda$) or from DC-regime (when $\Omega > 1/\lambda$). By contrast, in thick films B-type regimes can be observed provided $\Omega < \lambda$ (see Fig. 5a). Equations of all the boundaries between the regimes in figure 5 are given in table II.

Table II. — *Equations of boundaries between the regimes on the kinetic diagram in figure* 5.

Regime/regime	Equation	Regime/regime	Equation
C/B	$\tau = 1$	C/E	$\tau = \lambda^2$
DC/DB	$\tau = 1$	B/E	$\tau = \lambda^4$
C/DC	$\tau = 1/\Omega^2$	DC/E	$\tau = \lambda/\Omega$
B/DB	$\tau = 1/\Omega^4$	DB/E	$\tau = \lambda^2/\Omega^2$

Noteworthy, if the reduced drift velocity Ω falls below 1/2, the driven regimes DC and DB can be no longer observed. Therefore, $\Omega < 1/2$ can be considered as a quantitative criterion of purely diffusion (drift-free) transport of the tracer. In natural variables, this inequality reduces to $V_e < V_c \equiv D'/L(0)$. For the interstitial mechanism of oxygen transport, using estimated value of V_e from equation (37) we get $V_e/V_c \simeq (1 + z)/f'$, which shows that V_e is of the same order of magnitude as V_c or, at least, not so much higher. Then, at most weakly driven tracer transport can be expected to occur, if not pure diffusion. However, for the vacancy mechanism V_e is much greater than the right-hand side of equation (37), due to which the ratio V_e/V_c is considerably higher. In this case, therefore, strongly driven transport of ^{18}O can be very probably observed in experiments.

5. Conclusions.

Interpretation of ^{18}O profiles measured in « double-oxidation » experiments was hitherto based on the spherical-grain model [7, 20], which was earlier proposed for GB diffusion in metals [21] and oxides [22]. In part I of this paper [1] we have proposed an alternative model based on parallel GBs geometry (see Fig. 1). As was discussed in reference [1], this model has certain advantages over the spherical model. In particular, this model enables one to apply theoretical ideas and mathematical techniques previously developed for Fisher's model of GB diffusion [2-6, 8, 9, 14, 15, 18] and GB electromigration theory [9-13]. In part I, basic assumptions of the model have been discussed in detail and complete mathematical formulation of the model has been presented. However, the further analysis in reference [1] was restricted to the type A regime (higher temperatures) and the type C regime (lower temperatures).

In this paper, part II, we have extended the analysis to type B diffusion conditions, which is an intermediate case between C-regime and A-regime. When the GB penetration depth L' is not so large (i.e. $\ll L(0)$), the basic equations of the present model are formally the same

as those for GB electromigration. Using this analogy, we have derived the exact analytical solution of the basic equations (Eq. (20)). Moreover, taking advantage of the Efros theorem in Laplace transformation theory, we have found a much simpler integral representation of the solution compared to that given in reference [12]. In particular, our solution (20) does not include the Bessel functions and is much more suitable for numerical calculations. Figure 4 shows typical ^{18}O penetration profiles (more exactly, their portions caused by GB transport) as calculated from the exact analytical solution.

What is also important, the solution obtained is rather general and includes C-type and B-type conditions as particular cases. While analyzing limiting cases of this solution, we have come to the conclusion that there can be four kinetic regimes of oxygen tracer transport along GBs : along with the normal B-regime and C-regime, one can also observe a strongly driven B-type regime (DB-regime) and a strongly driven C-type regime (DC-regime). The kinetic diagram in figure 3 represents velocity-time conditions of realizing the regimes. The regimes differ in the penetration law (L' as a function of time (see Tab. I)) and the shape of the profile (see Figs. 2 and 4). Accordingly, methods of profile processing for diffusion parameters determination are also different. Strongly driven regimes, DC and DB, are more likely to be found at lower temperatures, especially under the vacancy mechanism of oxygen transport.

Since the oxide film has a finite thickness, a moment comes when the tracer penetrating along GBs reaches the oxide/metal interface and spreads over it. Since this moment, a second isotope peak can appear as a result of backward lattice diffusion as well as tracer incorporation in growing oxide layers. Later on, GBs remain in isotope equilibrium and act as tracer sources in the diffusion-controlled $^{18}O/^{16}O$ exchange occurring in the bulk. A generalized kinetic diagram taking into account the finite size effect and the transition to GB isotope equilibrium (E-regime) is represented by figure 5. In fact, there can be two different types of this diagram, figures 5a and 5b, depending on the film thickness $L(0)$. For thick films ($L(0) > L_*$) and thin films ($L(0) < L_*$) the regimes observed and their durations are essentially different. The critical thickness L_* is determined by equation (42) and depends on the temperature, as well as on the oxide type. To feel the quantities, it is not unreasonable to assume that typically $D'/D \simeq 10^4$ to 10^8. Then, with $\delta = 0.5$ nm, we have $L_* \simeq 0.02$ to 2 μm, which is within the working range of film thicknesses in oxidation experiments.

Finally, it should be admitted that figures 2, 3 and 5 are highly schematical since in reality all the quantities involved can vary by orders of magnitude. Nevertheless, these sketches give a right qualitative idea of what is going on during the oxygen tracer penetration, which can be helpful in designing « double-oxidation » experiments and interpreting their results.

Acknowledgements.

The authors are grateful to Dr J. Jedlinski and Dr W. Wegener for fuitful discussions. The work was supported by the Deutsche Forschungsgemeinschaft.

References

[1] MISHIN Yu. M. and BORCHARDT G., *J. Phys. III France* **3** (1993) 863.
[2] FISHER J. C., *J. Appl. Phys.* **22** (1951) 74.
[3] WHIPPLE R. T. P., *Philos. Mag.* **45** (1954) 1225.
[4] KAUR I. and GUST W., Fundamentals of Grain and Interphase Boundary Diffusion (Ziegler Pres Stuttgart, 1988).

[5] MISHIN Yu. M. and RAZUMOVSKII I. M., *Acta Metall. Mater.* **40** (1992) 597.
[6] HARRISON L. G., *Trans. Faraday Soc.* **57** (1961) 1191.
[7] BASU N. S. and HALLORAN J. W., *Oxid. Met.* **27** (1987) 143.
[8] LE CLAIRE A. D., *Brit. J. Appl. Phys.* **14** (1963) 351.
[9] GUPTA D., CAMPBELL D. R. and HO P. S., Thin Films : Interdiffusion and Reactions, J. M. Poate, K. N. Tu and J. W. Mayer Eds. (Wiley, NY, 1978) p. 195.
[10] MARTIN G., Phys. Status Solidi (A) **14** (1972) 183.
[11] TAI K. L., SUN P. H. and OHRING M., *Thin Solid Films* **25** (1975) 343.
[12] TAI K. L. and OHRING M., *J. Appl. Phys.* **48** (1977) 28.
[13] TAI K. L. and OHRING M., *J. Appl. Phys.* **48** (1977) 36.
[14] MISHIN Yu. M. and YUROVITSKII I. V., *Philos. Mag. A* **64** (1991) 1239.
[15] MISHIN Yu. M. and RAZUMOVSKII I. M., *Acta Metall. Mater.* **40** (1992) 839.
[16] LAVRENTIEV M. A. and SHABAT V. B., Functions of Complex Variables : Theory and Methods (Nauka Publishers, Moscow, 1973) p. 513 (in Russian).
[17] ABRAMOWITZ M. A. and STEGUN I. A., Handbook of Mathematical Functions, U.S. Dept. of Commerce (Washington, D.C., 1964) p. 298.
[18] MISHIN Yu. M., *Phys. Status Solidi (A)* **129** (1992) 101.
[19] KOFSTAD P., High Temperature Corrosion (Elsevier Applied Science, Lond.-NY, 1988).
[20] WEGENER W. and BORCHARDT G., *Oxid. Met.* **36** (1991) 339.
[21] BOKSHTEIN B. S., MAGIDSON I. A. and SVETLOV I. L., *Phys. Met. Metallogr.* **6** (1958) 81.
[22] OISHI Y. and ICHIMURA H., *J. Chem. Phys.* **71** (1979) 2281.